JACS
JOURNAL OF THE AMERICAN CHEMICAL SOCIETY
Article
pubs.acs.org/JACS

# The Importance of Attractive Three-Point Interaction in Enantioselective Surface Chemistry: Stereospecific Adsorption of Serine on the Intrinsically Chiral Cu{531} Surface

Tugce Eralp,[†] Alex Ievins,[‡] Andrey Shavorskiy,[†] Stephen J. Jenkins,[‡] and Georg Held*[,†]

[†]Department of Chemistry, The University of Reading, Whiteknights, Reading, RG6 6AD, United Kingdom
[‡]Department of Chemistry, University of Cambridge, Lensfield Road, Cambridge, CB2 1EW, United Kingdom

Supporting Information

**ABSTRACT:** Both enantiomers of serine adsorb on the intrinsically chiral Cu{531} surface in two different adsorption geometries, depending on the coverage. At saturation, substrate bonds are formed through the two oxygen atoms of the carboxylate group and the amino group ($\mu$3 coordination), whereas at lower coverage, an additional bond is formed through the deprotonated $\beta$-OH group ($\mu$4 coordination). The latter adsorption geometry involves substrate bonds through three side groups of the chiral center, respectively, which leads to significantly larger enantiomeric differences in adsorption geometries and energies compared to the $\mu$3 coordination, which involves only two side groups. This relatively simple model system demonstrates, in direct comparison, that attractive interactions of three side groups with the substrate are much more effective in inducing strong enantiomeric differences in heterogeneous chiral catalyst systems than hydrogen bonds or repulsive interactions.

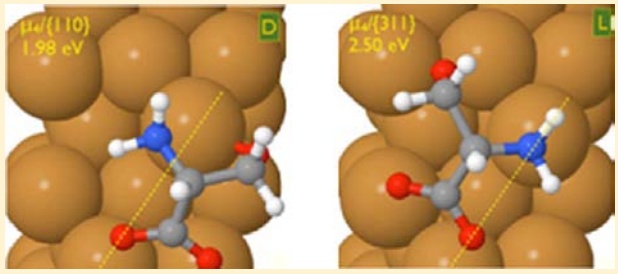


## INTRODUCTION

It has been long recognized that chiral recognition requires a three-point interaction of the reactant molecule, i.e., three side groups of the chiral center have to be held in place by specific interactions with its environment, either attractive or repulsive.[1,2] This implies one of the biggest challenges in designing heterogeneous enantioselective catalysts: a two-dimensional solid surface needs to be functionalized such that it confines the three side groups of a chiral (or prochiral) molecule, which are not normally accessible in the same plane. So far, the most successful strategies for achieving this goal involve "adding a third dimension" to the catalyst surface, either by tethering homogeneous catalyst molecules, which provide all three interactions,[3] or by employing large modifier molecules, which create a stereoselective environment together with the surface.[4,5] The mechanisms for these systems are relatively well understood. In addition, enantioselectivity has also been observed on intrinsically chiral model catalysts, i.e., single crystal metal surfaces without mirror symmetry, which are not superimposable onto their mirror images.[6−8] In the past, these observations have been largely qualitative using temperature programmed desorption (TPD)[6] or cyclovoltammetry[7] to demonstrate enantiomeric differences. More detailed information about the number and nature of interactions with the metal surface only emerged over the past few years, both from theory and experiment.[9−14] So far, however, it was not possible to identify the type of bonds necessary to induce enantioselectivity in such adsorption systems.

Here we concentrate on the adsorption of serine on the intrinsically chiral Cu{531} surface (see Figure 1). In contrast to glycine and alanine,[12,14] serine can form bonds with the Cu surface through either two or three side groups of the chiral center, depending on coverage. Therefore, this model system allows a direct comparison in terms of enantioselectivity between different levels of coordination. We show that attractive interactions of three side groups of the chiral center are critical for large enantiomeric differences in the adsorption geometries and energies. The enantiomeric differences are much weaker if only two side groups are involved in surface bonds and the third interaction is either repulsive or through weak hydrogen bonds. In the latter case, the adsorption "footprint" is similar to alanine, and also the magnitude of enantiomeric differences is comparable.

## EXPERIMENTAL AND COMPUTATIONAL PROCEDURES

**Experimental Procedures.** The experiments were performed in two different ultrahigh vacuum (UHV) chambers. Sample preparation, preliminary TPD and low-energy electron diffraction (LEED) experiments were performed at the University of Reading. The majority of the experiments reported here were carried out at the UE52-PGM end-station of the German synchrotron radiation facility BESSY, which was equipped with a partial yield detector for near edge X-ray absorption fine structure (NEXAFS) measurements and a hemispherical electron energy analyzer used for X-ray photoelectron

**Received:** November 8, 2011
**Published:** May 14, 2012

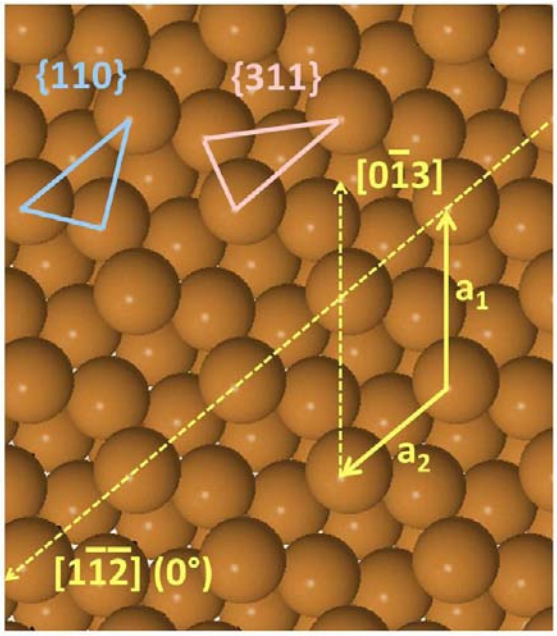


**Figure 1.** Ball model of the clean unreconstructed Cu{531}$^S$ surface indicating the surface unit cell vectors and the main crystallographic directions. The unit cell contains two Cu atoms, in the first and second layer, which can be involved in bonds with adsorbed amino acids. At the top of the diagram {110} and {311} microfacets are indicated, which consist of two first layer Cu atoms and one second layer atom forming rectangular and isosceles triangles, respectively. The Cu{531}$^R$ surface is the mirror image of Cu{531}$^S$.

spectroscopy (XPS). For all experiments the base pressure was in the $10^{-10}$ mbar range. Two well characterized Cu{531} samples with *R* and *S* chirality, respectively, were used for the experiments at Reading and BESSY. The sample temperature was measured through a thermocouple attached to the sample holder. The samples were cleaned using standard procedures.[14,15] L- and D-serine (purity ≥99%, from Sigma-Aldrich) were deposited from a home-built evaporator source held at 160 °C.[16] The enantiomers were from the same source and batches as those used to study serine adsorption on the achiral Cu{110} surface,[16] where they show perfect mirror behavior at every level of structural detail. It can, therefore, be excluded that major enantiomeric differences on Cu{531} could be induced by different levels/types of impurities of the two enantiomers. Throughout the text we use notations like "L-serine on Cu{531}$^R$ (D-serine on Cu{531}$^S$)" when necessary in order to account for the fact that chiral surface systems are equivalent when, both adsorbate and substrate chiralities, are inverted together. The substrate/adsorbate combination in brackets is the system equivalent to the one for which the experiments or calculations have been performed.

The relative adsorbate coverage was determined by comparing the area of the XPS peaks with those of the saturated chemisorbed layer. C 1s, N 1s, and O 1s XP spectra were measured with a photon energy of 630 eV. The binding energy (BE) scale was calibrated with respect to the Fermi energy, which was determined using the same beamline and analyzer settings as for the core level spectra. All NEXAFS experiments were performed at normal incidence. The in-plane polarization of the X-ray beam could be changed continuously between horizontal (∥ [11$\bar{2}$]) and vertical orientation. C K-edge NEXAFS spectra were recorded in the partial-yield mode while scanning the photon energy from 286 to 320 eV. The spectra shown here are normalized with respect to the photon flux and have the background spectra of the clean surface subtracted. Details of the NEXAFS data analysis are described in the Supporting Information and in refs 12 and 14.

For the laboratory experiments, a low current LEED instrument (Omicron NanoTechnology) was used to record the diffraction patterns. Using primary beam currents ∼100 nA, no significant beam damage was observed over a period of ∼30 min. Each LEED experiment was followed by TPD, measuring the decomposition products, $H_2$ (mass 2) and $CO_2$ (mass 44), to determine the relative coverage.

**DFT Model Calculations.** DFT geometry optimizations were performed using the CASTEP DFT code.[17] The generalized gradient approximation (GGA) method (PW91)[18] and ultrasoft pseudopotentials[19] were employed to account for effects of exchange and correlation and to mimic the core electron behavior. A plane-wave basis set truncated at 340 eV was used with a Monkhorst–Pack mesh[20] to sample points for integration within the Brillouin zone. All surface calculations employed a 2×3×1 *k*-point mesh for the (−1 1; −1 −2) unit cell and a 22-layer Cu{531}$^S$ slab, the lower half of which was constrained in bulk positions with a lattice constant of 3.606 Å. A vacuum spacing equivalent to 21 layers (∼13.4 Å) separated the metal slabs. Positive adsorption energies were calculated according to

**Table 1. Summary of the DFT and NEXAFS Results**[a]

| | adsorption energy | $\alpha_{DFT}$ | $\alpha_{exp}$ (coverage) |
|---|---|---|---|
| | L-Serine | | |
| {110} $\mu$3 $\beta$-OH intact | 2.00 | 38° | 31° (100% sat/0.50 ML) |
| {311} $\mu$3 $\beta$-OH intact | 1.71 | −30° | −28° (100% sat/0.50 ML) |
| {110} $\mu$4 $\beta$-OH intact | 2.00 | 52° | |
| {311} $\mu$4 $\beta$-OH intact | 1.90 | −13° | |
| {110} $\mu$4 $\beta$-OH deprotonated | 1.98 | 80° | |
| {311} $\mu$4 $\beta$-OH deprotonated | **2.50** | −10° | −14° [b] (52% sat/0.26 ML) |
| | D-Serine | | |
| {110} $\mu$3 $\beta$-OH intact | 2.00 | 47° | 35° (100% sat/0.50 ML) |
| {311} $\mu$3 $\beta$-OH intact | 1.68 | −44° | −23° (100% sat/0.50 ML) |
| {110} $\mu$4 $\beta$-OH intact | 1.87 | 37° | |
| {311} $\mu$4 $\beta$-OH intact | 1.77 | −61° | |
| {110} $\mu$4 $\beta$-OH deprotonated | **1.98** | 30° | 24° (59% sat/0.30 ML) |
| {311} $\mu$4 $\beta$-OH deprotonated | 1.74 | −78° | |

[a]Adsorption energies (eV) found for different configurations of L- and D-Ser on Cu{531}$^S$ are listed together with the orientation angle $\alpha$ calculated for each configuration ($\alpha$ is the angle between the [11$\bar{2}$] direction and the surface projection of the normal of the carboxylate O–C–O triangle). These are compared with the experimental angles extracted from NEXAFS (only majority species for low-coverage L-serine). [b]−14° is the value found for a fit to the L-serine data with one molecular orientation. If two angles are allowed, the mean value is −16° ± 3°. See text and Supporting Information for details.


dx.doi.org/10.1021/ja210499m | J. Am. Chem. Soc. 2012, 134, 9615–9621

$$G_{ads} = H(\text{Ser(gas)}, T = 0, p = 0) + H(\text{Cu}\{531\}) - H(\text{Ser/Cu}\{531\}) - n\mu(\text{H}_2, T, p) \quad (1)$$

where $n = 1/2$ or 1 for serine with an intact or deprotonated $\beta$-OH group, respectively (in all cases the carboxylic acid group is assumed to be deprotonated). The gas-phase optimizations of intact serine and hydrogen were performed within a $10 \times 10 \times 10$ Å$^3$ cubic supercell. The chemical potential of $H_2$ was included for a more reliable comparison between the different chemical forms:

$$\mu(\text{H}_2, T, p) = kT\ln\left(\frac{p}{p^0}\right) + \frac{1}{N_A}(H(\text{H}_2, 0, 0) + \Delta H(\text{H}_2, 0 \rightarrow T, p^0)) - TS(\text{H}_2, T, p^0) \quad (2)$$

with values of $\Delta H$ and $S$ taken from experimental data.[21] The adsorption energies listed in Table 1 are those for $T = 298.15$ K and $p = 10^{-10}$ mbar.

The added computational cost resulting from the larger unit cell of L-serine on Cu{531}$^S$ (D-serine on Cu{531}$^R$) that is observed experimentally made it necessary to carry out this optimization also in the smaller (−1 1; −1 −2) unit cell of D-serine. This is an approximation, but it also allows a better comparison between the two enantiomers. The complexity of the structures means that finding the global adsorption energy maximum in each case is a severe challenge. Although excellent agreement with the experimental data was achieved for the lower coverage structures, the values must be taken as lower bounds.

## RESULTS

When serine is deposited at room temperature no condensation of multilayers is observed, as indicated by the saturation of peak areas in both XPS and TPD experiments (not shown). Electron diffraction gives a first indication of enantiomeric differences as different diffraction patterns are observed for the two enantiomers (see Figure 2). After annealing to 370 K, $p(1\times8)$ and $p(1\times4)$ diffraction patterns are observed for the saturated chemisorbed layers of L- and D-serine, respectively, on Cu{531}$^R$), as shown in Figure 2a (D- and L-serine, respectively, on Cu{531}$^S$). Faint elongated superstructure spots indicate nonperfect long-range order at this coverage. The bulk-terminated Cu{531} surface unit cell contains two Cu atoms, in the first and second layer, which can form bonds with adsorbate molecules (see Figure 1). Therefore, the $p(1\times4)$ unit cell can accommodate a maximum of two molecules if either three or four molecule−Cu bonds are formed, which leads to a relative coverage of 2/4 = 0.50 ML at saturation (1 ML corresponds to 1 molecule per (1×1) surface unit cell; note that the {531} unit cell has a significantly larger area than those of close-packed surfaces, cf. Figure 1). The fact that a smaller surface unit cell is observed for lower coverages (see below) excludes the possibility of having only one molecule per unit cell at saturation coverage. Two molecules per $p(1\times4)$ unit cell also imply that, both {110} and {311} microfacet adsorption sites, are equally occupied.[12] The comparison of XPS and TPD peak areas shows that the saturation coverage is the same for both enantiomers. Between 30% and 60% of saturation coverage (∼0.15−0.30 ML), the two enantiomers show diffraction patterns indicating (−1 1; −1 −2) and (−1 1; −2 −4) superstructures for L- and D-serine on Cu{531}$^R$ (D- and L-serine on Cu{531}$^S$), which correspond to a nominal coverage of 0.33 ML (see Figure 2b). Unlike for the saturated layers, ordering of the low-coverage layers occurs already at room temperature.

Note that the LEED experiments were performed on a Cu{531}$^R$ surface. As discussed above, on the Cu{531}$^S$ surface, which was used for the XPS and NEXAFS experiments and the DFT calculations, one would therefore expect the superstuctures reported here for the opposite serine enantiomers.

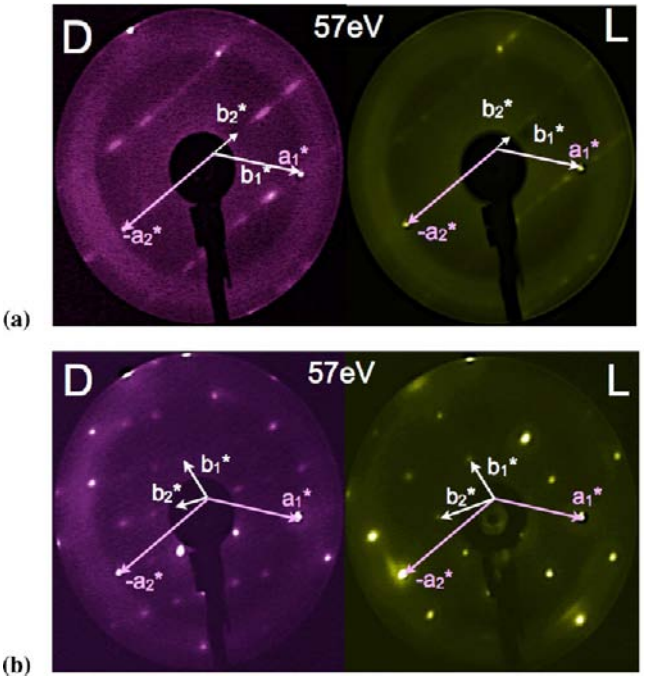


**Figure 2.** LEED superstructures observed at 57 eV for (a) saturation coverages (0.50 ML) of D- and L-serine and (b) 52% (0.26 ML) and 58% (0.29 ML) of saturation coverage of D- and L-serine, respectively, on Cu{531}$^R$ (L- and D-serine on Cu{531}$^S$). Clean surface ($a_1$* and $a_2$*) and overlayer ($b_1$* and $b_2$*) reciprocal unit cell vectors are included in the images.

The C 1s and N 1s XP spectra are similar to those observed for serine on Cu{110}[16] and show little qualitative differences when the coverage or the enantiomer changes. In particular, the N 1s spectra show a single main peak near BE 400 eV, which indicates that the amino group is involved in a surface bond at all coverages[12,14,16,23,24] (see also Supporting Information). In the O 1s region, however, large changes occur as the coverage of either enantiomer increases (Figure 3). At all coverages the main peak is observed around 531.4 eV. Narrow O 1s peaks at this binding energy (BE) have been observed for a number of amino acids on Cu surfaces and are assigned to the two oxygen atoms of the deprotonated carboxylate group, each forming a bond with a Cu atom.[12,14,22−24] For low coverage, up to ∼0.3 ML, a shoulder at the low BE side (530.8 eV) is observed, which is assigned to the $\beta$-OH group. The area ratios between the main peak and the shoulder are 2.5 and 2.2 for L- and D-serine on Cu{531}$^S$, which is close to expected ratio of 2:1 within the margin of fluctuations induced by photoelectron diffraction effects. The low BE of the shoulder indicates that this oxygen atom is also deprotonated and bound to the substrate resulting in a total of four covalent bonds with the substrate, whereby three side groups of the chiral center are involved in attractive substrate interactions (amino, carboxylate, and $\beta$-OH). Using a nomenclature adapted from organometallic compounds, we refer to this adsorption complex as an overall $\mu4$ configuration (four covalent bonds with the substrate).[24]


dx.doi.org/10.1021/ja210499m | J. Am. Chem. Soc. 2012, 134, 9615−9621

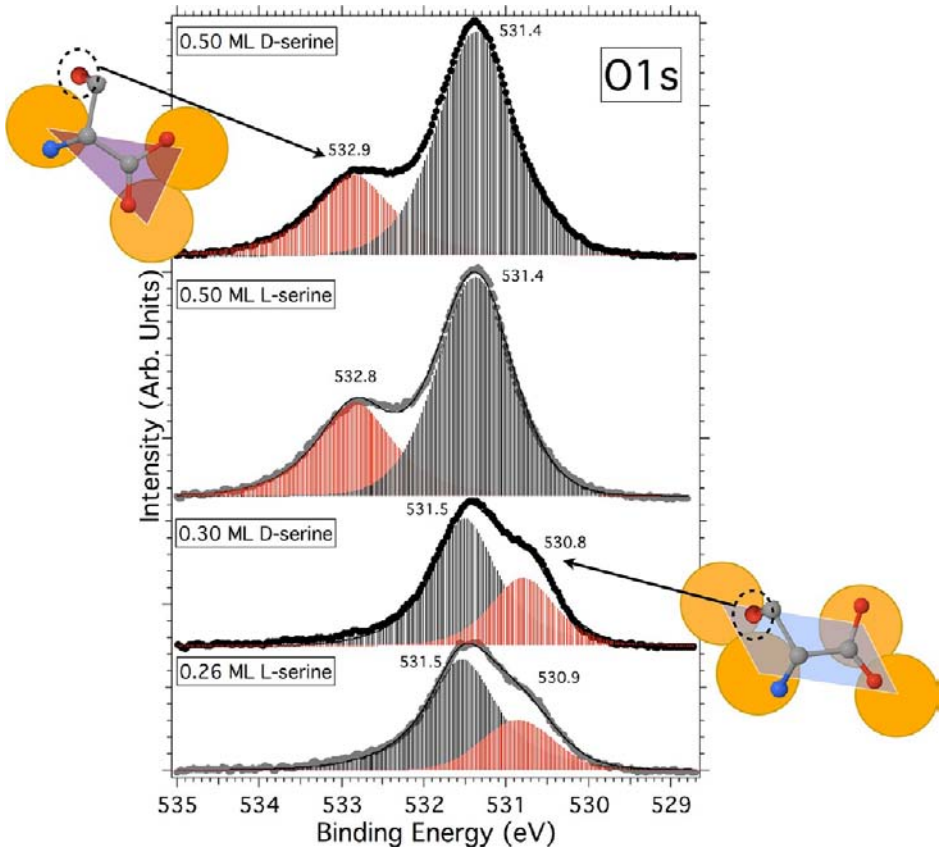


**Figure 3.** O 1s XP spectra of different coverages of L- and D-serine adsorbed on Cu{531}$^S$ (photon energy = 630 eV). The insets indicate the likely adsorption–bond coordination. For clarity, hydrogen atoms are omitted in the diagrams.

When the coverage approaches saturation, the low BE shoulder disappears, and a new peak appears at 532.8 eV, with area ratios of 1:2.1 and 1:2.4 compared to the main peak for L- and D-serine on Cu{531}$^S$. This BE is typical for $\beta$-OH groups not bound to the metal surface, as in the case of serine on Cu{110}.[16] Therefore we conclude that the $\beta$-OH group is not bound to the surface for the higher coverage. This means that the molecule forms a $\mu$3 substrate bond, but the $\beta$-OH group can still be involved in intermoleculer hydrogen bonds. The transition between $\mu$4 and $\mu$3 occurs at similar coverage for both enantiomers and appears to be driven by steric constraints. The $\mu$4 substrate bond has a larger footprint than the high-coverage $\mu$3 bond. Hence, the surface can accommodate more molecules in the latter configuration.

In contrast to the XPS data, the NEXAFS data show strong enantiomeric differences. The carbon K-edge NEXAFS spectra of low-coverage and saturated chemisorbed layers of L- and D-serine on Cu{531}$^S$ show sharp resonances at 289 eV, which are assigned to the carboxylate $\pi$-system[22,25] (spectra shown in the Supporting Information). According to the dipole selection rule, the $\pi$-resonance intensity of a single molecule varies like $\cos^2\alpha$, depending on the angle $\alpha$ between the polarization vector and the normal to the plane of the O–C–O carboxylate group.[26] The measured angular dependence can, therefore, be used to determine the orientation of the molecules.[8,12,14,22] The data sets for the saturated layers of D- and L-serine on Cu{531}$^S$ (Figure 4a,b) are very similar. The intensity reaches a nonzero minimum, which indicates, that the molecules assume at least two orientations. The angular dependence is also similar to glycine and alanine, which occupy adsorption sites on the {311} and {110} microfacets of Cu{531} (see Figure 1) with two different orientations.[12,14] At half saturation, the two enantiomers show very significant differences. The data sets for half saturation (0.26 and 0.30 ML) and saturation coverage were initially fitted allowing two orientations, characterized by the angles $\alpha_1$ and $\alpha_2$ with respect to the $[11\bar{2}]$ direction (see Figure 1) and variable relative occupations. For saturation coverage ($\mu$3-bond), the relative occupations $A_{1,2}$ were only varied within narrow limits around $A_2$:$A_1$ = 1 ± 30% as this is the only way of packing 2/4 molecules with 3 surface bonds each into a $p(1\times4)/p(1\times8)$ unit cell. The fit results are included in the graphs of Figure 4 (for details see Supporting Information). The best-fit orientation angles of the two enantiomers differ by ~5° ($\alpha_1$ = −28/−23°; $\alpha_2$ = −31/−35° for L-/D-serine on Cu{531}$^S$), which is within the estimated error margin of ±10°. For the low-coverage $\mu$4 configuration, however, there is a clear preference for only one orientation, and the enantiomeric difference between the orientations of the majority species is significantly greater (Figure 4c,d). The data for D-serine on Cu{531}$^S$ can only be fitted when all molecules are in the same orientation, $\alpha_1$ = 24°. Assuming one orientation for the 0.26 ML L-serine data leads to $\alpha_1$ = −14°. This orientation is rotated by −38° with respect to the D-enantiomer. Allowing two angles leads to the same level of agreement for $\alpha_1/\alpha_2$ values at similar occupation numbers, which are displaced by up to 15° in opposite directions from a mean value around −16° ± 3°. Two orientations with similar occupation for L-serine on Cu{531}$^S$ are compatible with the fact that a larger unit cell, (−1 1; −2 −4), is observed in LEED (D-serine on Cu{531}$^R$), which contains two molecules. In this

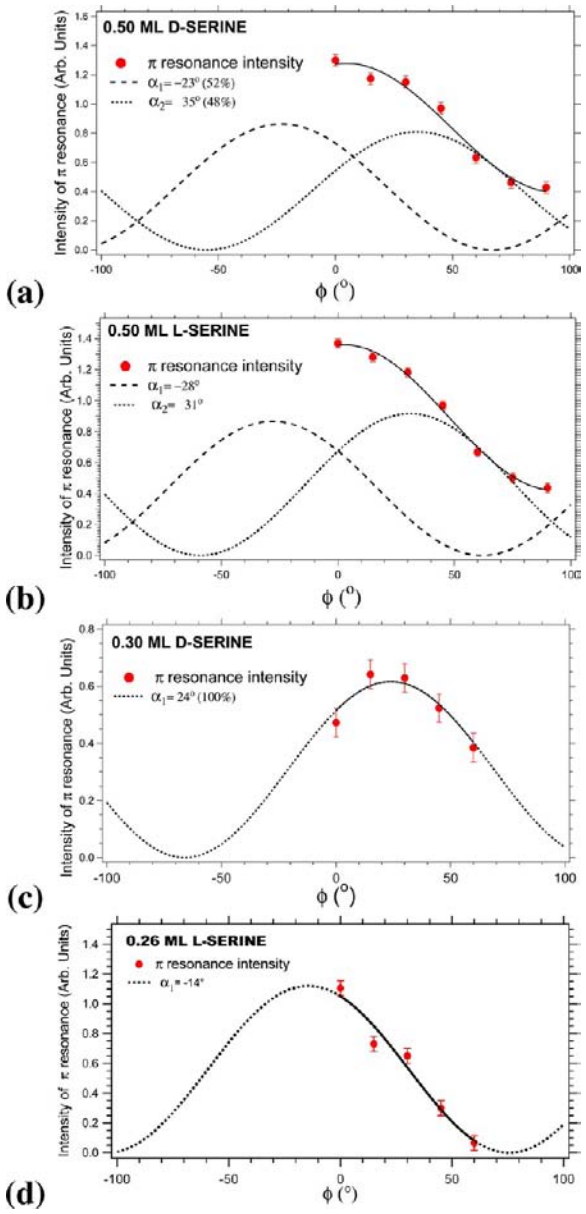


**Figure 4.** Angular dependence of the $\pi$-resonance in the NEXAFS spectra of the saturation coverages (0.50 ML) of L- and D-serine (a, b), 0.30 ML D-serine (c), and 0.26 ML L-serine (d) on Cu{531}$^S$. The fitted angular dependence (individual orientations and sum of the two curves) and the parameters $\alpha_{1,2}$ of the best fits are included in the diagrams.

case, however, only their mean orientation can be determined with sufficient accuracy from the NEXAFS data.

Structural optimizations based on DFT were performed for the low-coverage geometries of D- and L-serine on Cu{531}$^S$ in three different adsorption states ($\mu$3 and $\mu$4 with intact $\beta$-OH group and $\mu$4 with deprotonated $\beta$-OH group) and two adsorption sites involving the {110} and {311} microfacets, respectively. The adsorption energies are listed in Table 1, and the optimized structures are shown in Figure 5. L-serine shows a clear preference for $\mu$4 adsorption on the {311} microfacet with deprotonated $\beta$-OH, while two structures of D-serine, $\mu$3 and $\mu$4 with intact and deprotonated $\beta$-OH, respectively, on the {110} facet, have almost identical adsorption energies. The $\mu$3 structure leads to a slightly higher calculated adsorption energy, by 0.02 eV, but the $\mu$4 geometry is in much better agreement with the experimental data for low-coverage adsorption and must, therefore, be considered as the preferred one. The small energy difference between the two structures is well within the typical error bars of DFT. We therefore conclude that, both L- and D-serine, assume $\mu$4 adsorption geometries with deprotonated $\beta$-OH side groups but on different microfacets, {311} and {110}, respectively. The molecular orientations in these structures are in excellent agreement with those of the majority species at low coverage derived from the NEXAFS data, which are also listed in Table 1.

## DISCUSSION AND CONCLUSION

Preferences for certain adsorption geometries are driven by a balance between the chemical interaction with the substrate and conformational strain. Both depend on the number of surface bonds and the type of microfacet. Figure 5 shows significant structural differences between the $\mu$4 adsorption geometries of the two enantiomers. These are most pronounced for the deprotonated geometries on the {311} microfacet, where the proximal first- and second-layer copper atoms (left and middle atom in the top row) provide the necessary support for a strong bridge bond of the $\beta$-OH group of L-serine on Cu{531}$^S$, whereas only one second layer Cu atom is available for D-serine on the same site (bottom right), which leads to increased conformational strain. Candidate substrate atoms are not as proximal for the deprotonated geometries on the {110} facet so that somewhat increased Cu−O/N bond lengths, the sharing of a Cu atom between the $\beta$-OH and the amino group in the case of D-serine, and additional conformational strain outweigh the benefits of increased binding. This renders the adsorption energies almost equal—despite major differences in the substrate bonds—and very similar to $\mu$3 binding. In all deprotonated $\mu$4 geometries the Cu−O/N bond lengths are ∼2.0 Å (between 1.86 and 2.09 Å), i.e., in the range of strong covalent bonds. The effect of an intact $\beta$-OH group in the $\mu$4 geometries is a dramatic increase in the respective Cu−O bond length by at least 0.3 Å, which weakens this substrate bond significantly. In addition to the enantiomeric differences at the molecular level there are also significant differences in the global organization as the superlattices of the two enantiomers. For the $\mu$4 configuration, the (−1 1; −2 −4) unit cell of L-serine is twice as big as the (−1 1; −1 −2) unit cell of D-serine (on Cu{531}$^S$) and therefore contains two molecules with different orientations. This is likely to be related to the fact that the adsorption geometry allows hydrogen bonding between one of the carboxylate oxygens (far left in Figure 5) and the $NH_2$ group of a neighboring molecule. The NEXAFS data for L-serine are compatible with orientations of the two molecules which oscillate around a mean orientation (∼ −16°) close to the orientation predicted by DFT for the smaller (−1 1; −1 −2) unit cell.

For the $\mu$3 geometries, where only two side groups form bonds, enantiomeric differences in adsorption energies and the footprints of the substrate bonds are minimal. The weak interaction of the $\beta$-OH group with the substrate leads to small differences in the molecular orientations, which are in qualitative agreement with the experimental findings for saturation coverage. Bigger discrepancies between the theoretical and experimental angles are to be expected for higher coverage since all calculations were carried out assuming a (−1 1; −1 2) overlayer (0.33 ML) with a separation of more than 6.75 Å between the adsorption sites and a minimum


dx.doi.org/10.1021/ja210499m | J. Am. Chem. Soc. 2012, 134, 9615−9621

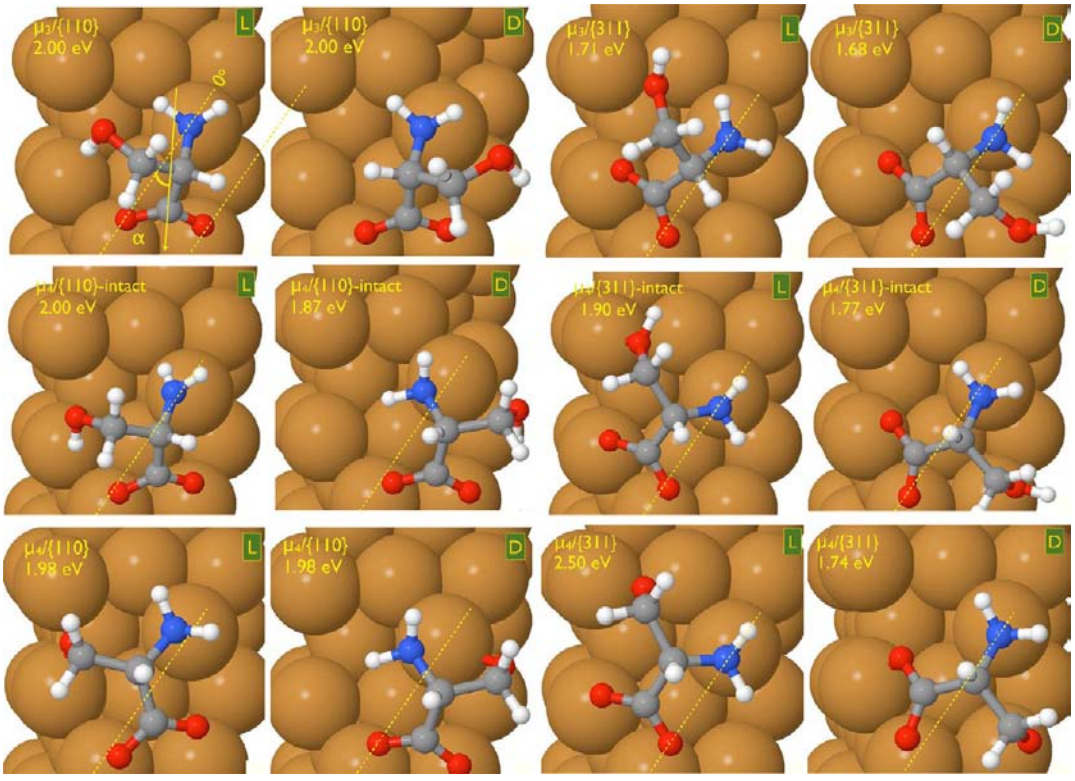


**Figure 5.** DFT-optimized $\mu$3 and $\mu$4 adsorption geometries for L- and D-serine on the {110} and {311} microfacets of Cu{531}$^S$; top to bottom: $\mu$3 with intact $\beta$-OH, $\mu$4 with intact $\beta$-OH, $\mu$4 with deprotonated $\beta$-OH (red = oxygen, blue = nitrogen, gray = carbon, white = hydrogen). The respective adsorption energies are indicated in the figure. The dotted lines (0°) indicate the $[11\bar{2}]$ crystallographic direction.

distance of typically ~3 Å between adjacent atoms of neighboring molecules. Intermolecular repulsion and hydrogen bonding therefore play a minor role in determining the adsorption geometry at this low coverage, whereas these lateral interactions have a significant effect on the arrangement and adsorption energies of molecules at high coverage. In addition, the change from a $\mu$3 to a $\mu$4 geometry enables a higher coverage and, thus, a higher adsorption energy per surface area. This makes an equal $\mu$3 occupation of {110} and {311} adsorption sites at saturation coverage energetically favorable despite the clear energy difference at low coverage.

It is important pointing out that the adsorption geometries associated with {311} and {110} mircofacets are not necessarily comparable with the arrangement of molecules on the respective single crystal surfaces. Our recent study of serine on Cu{110}[16] showed dimer-like structures, which are the result of strong intermolecular hydrogen bonding, even at very low coverages. The same dimer building blocks could not be formed on the {110} facets of Cu{531} since each microfacet contains only one {110} unit cell, cf. Figure 1. On the other hand, the Cu{531} surface—unlike Cu{110}—provides adsorption sites that can accommodate unstrained $\mu$4 geometries, as discussed above. No spectroscopic evidence for $\mu$4 adsorption of serine at any coverage has been found on Cu{110}.

In summary, we show through a combination of XPS, NEXAFS, and DFT that both enantiomers of serine adsorb on Cu{531} in $\mu$4 geometries (with deprotonated $\beta$-OH groups) at low coverage, up to ~60% saturation, and in $\mu$3 geometries at saturation coverage. Significantly larger enantiomeric differences are seen in adsorption energies and molecular bonding for $\mu$4 geometries, which involve substrate bonds of three side groups of the chiral center, i.e., a three-point interaction. The $\mu$3 adsorption geometry, where only the carboxylate and amino groups form substrate bonds and the $\beta$-OH group is involved in intermolecular interactions, most likely through hydrogen bonds, leads to small differences in the molecular orientations with respect to the substrate but no qualitative enantiomeric differences. This relatively simple model system allows a direct comparison in terms of enantiospecificity between different levels of coordination. It demonstrates that attractive interactions of three side groups with the substrate are much more effective in inducing significant enantiomeric differences in chiral catalyst surfaces than hydrogen bonds or repulsive interactions. If strong bonds are formed between reaction products and the catalyst surface, this is, of course, detrimental to the activity of a catalysts. Amino acids, however, are often used as chiral modifiers and, therefore, not directly involved in the reaction. Modifiers restructure the catalyst surface and/or transmit enantioselectivity through intermolecular interactions. In both cases strong substrate bonds are an advantage.

## ■ ASSOCIATED CONTENT

### Ⓢ Supporting Information

C 1s and N 1s XP spectra and examples of NEXAFS spectra together with a detailed description of the NEXAFS data analysis. This material is available free of charge via the Internet at http://pubs.acs.org.

## ■ AUTHOR INFORMATION

### Corresponding Author

g.held@reading.ac.uk

### Notes

The authors declare no competing financial interest.

## ■ ACKNOWLEDGMENTS

The research leading to these results has received funding from the European Community's Seventh Framework Programme (FP7/2007-2013) under grant agreement no. 226716 and through the Marie Curie Early Stage Training Network "MONET" (no. MEST-CT-2005-020908). The authors would also like to acknowledge the support during the experiments provided by the staff of BESSY II, in particular Dr D. Batchelor.

## ■ REFERENCES

(1) Easson, L. H.; Stedman, E. *Biochem. J.* **1933**, *27*, 1257−1266.
(2) Davankov, V. A. *Chirality* **1997**, *9*, 99−102.
(3) Proctor, G. *Asymmetric Synthesis*; Oxford University Press: Oxford, U.K., 1997.
(4) Baiker, A. *J. Mol. Catal. A* **1997**, *115*, 473.
(5) Baiker, A. *J. Mol. Catal. A* **2000**, *163*, 205.
(6) McFadden, C. F.; Cremer, P. S.; Gellman, A. J. *Langmuir* **1996**, *12*, 2483.
(7) Attard, G. A. *J. Phys. Chem. B* **2001**, *105*, 3158.
(8) Held, G.; Gladys, M. J. *Top. Catal.* **2008**, *48*, 128−136.
(9) Fasel, R.; Wider, J.; Quitmann, C.; Ernst, K.-H.; Greber, T. *Angew. Chem. Int. Ed* **2004**, *43*, 2853−2856.
(10) Bhatia, B.; Sholl, D. S. *J. Chem. Phys.* **2005**, *122*, 204707.
(11) Greber, T.; Sljivancanin, Z.; Wider, J.; Hammer, B. *Phys. Rev. Lett.* **2006**, *96*, 056103.
(12) Gladys, M. J.; Stevens, A. V.; Scott, N. R.; Jones, G.; Batchelor, D.; Held, G. *J. Phys. Chem. C* **2007**, *111*, 8331−8336.
(13) Bhatia, B.; Sholl, D. S. *J. Chem. Phys.* **2008**, *128*, 144709.
(14) Eralp, T.; Zheleva, Z. V.; Shavorskiy, A.; Dhanak, V. R.; Held, G. *Langmuir* **2010**, *26*, 10918−10923.
(15) Ammon, C.; Bayer, A.; Steinrück, H. P.; Held, G. *Chem. Phys. Lett.* **2003**, *377*, 163−169.
(16) Eralp, T.; Shavorskiy, A.; Zheleva, Z. V.; Held, G.; Kalashnyk, N.; Ning, Y.; Linderoth, T. R. *Langmuir* **2010**, *26*, 18841−18851.
(17) Clark, S.; Segall, M.; Pickard, C.; Hasnip, P.; Probert, M.; Refson, K.; Payne, M. *Z. Kristallogr.* **2005**, *220*, 567.
(18) Perdew, J. P.; Chevary, J. A.; Vosko, S. H.; Jackson, K. A.; Pederson, M. R.; Singh, D. J.; Fiolhais, C. *Phys. Rev. B* **1992**, *46*, 6671−6687.
(19) Vanderbilt, D. *Phys. Rev. B* **1990**, *41*, 7892−7895.
(20) Monkhorst, H. J.; Pack, J. D. *Phys. Rev. B* **1976**, *13*, 5188−5192.
(21) Lide, D. R.; Frederikse, H. P. R. *Handbook of Chemistry and Physics*, 76th ed.; CRC Press: Boca Raton, 1995.
(22) Hasselström, J.; Karis, O.; Weinelt, M.; Wassdahl, N.; Nilsson, A.; Nyberg, M.; Petterson, L. G. M.; Samant, M. G.; Stöhr, J. *Surf. Sci.* **1998**, *407*, 221−236.
(23) Jones, G.; Jones, L. B.; Thibault−Starzyk, F.; Seddon, E. A.; Raval, R.; Jenkins, S. J.; Held, G. *Surf. Sci.* **2006**, *600*, 1924−1935.
(24) Barlow, S. M.; Louafi, S.; Le Roux, D.; Williams, J.; Muryn, C.; Haq, S.; Raval, R. *Surf. Sci.* **2005**, *590*, 243−263.
(25) Nyberg, J.; Hasselström, M.; Karis, O.; Wassdahl, N.; Weinelt, M.; Nilsson, A.; Petterson, L. G. M. *J. Chem. Phys.* **2000**, *112*, 5420−5427.
(26) Stöhr, J. *NEXAFS spectroscopy*, 2nd ed.; Springer Series in Surface Sciences; Springer: Berlin, Germany, 1996.